



Since January 2020 Elsevier has created a COVID-19 resource centre with free information in English and Mandarin on the novel coronavirus COVID-19. The COVID-19 resource centre is hosted on Elsevier Connect, the company's public news and information website.

Elsevier hereby grants permission to make all its COVID-19-related research that is available on the COVID-19 resource centre - including this research content - immediately available in PubMed Central and other publicly funded repositories, such as the WHO COVID database with rights for unrestricted research re-use and analyses in any form or by any means with acknowledgement of the original source. These permissions are granted for free by Elsevier for as long as the COVID-19 resource centre remains active.



Synthetic nanobody-functionalized nanoparticles for accelerated development of rapid, accessible detection of viral antigens

Xiahui Chen^{a,b,c,1}, Shoukai Kang^{d,e,1}, Md Ashif Iqbal^{a,b,c,1}, Zhi Zhao^{a,b,2}, Yuxin Pan^{d,e}, Jiawei Zuo^{a,c}, Liangcai Gu^{d,e,**}, Chao Wang^{a,b,c,*}

^a School of Electrical, Computer and Energy Engineering, Arizona State University, Tempe, AZ, 85287, USA

^b Center for Molecular Design and Biomimetics at the Biodesign Institute, Arizona State University, Tempe, AZ, 85287, USA

^c Center for Photonic Innovation, Arizona State University, Tempe, AZ, 85287, USA

^d Department of Biochemistry, University of Washington, Seattle, WA, 98195, USA

^e Institute for Protein Design, University of Washington, Seattle, WA, 98195, USA

ARTICLE INFO

Keywords:

Infectious diseases
Co-binding nanobodies
Ebola virus
COVID-19
Metal nanoparticles
Rapid electronic detection

ABSTRACT

Successful control of emerging infectious diseases requires accelerated development of fast, affordable, and accessible assays for wide implementation at a high frequency. This paper presents a design for an in-solution assay pipeline, featuring nanobody-functionalized nanoparticles for rapid, electronic detection (Nano2RED) of Ebola and COVID-19 antigens. Synthetic nanobody binders with high affinity, specificity, and stability are selected from a combinatorial library and site-specifically conjugated to gold nanoparticles (AuNPs). Without requiring any fluorescent labelling, washing, or enzymatic amplification, these multivalent AuNP sensors reliably transduce antigen binding signals upon mixing into physical AuNP aggregation and sedimentation processes, displaying antigen-dependent optical extinction readily detectable by spectrometry or portable electronic circuitry. With Ebola virus secreted glycoprotein (sGP) and a SARS-CoV-2 spike protein receptor binding domain (RBD) as targets, Nano2RED showed a high sensitivity (the limit of detection of ~ 10 pg/mL, or 0.13 pM for sGP and ~ 40 pg/mL, or ~ 1.3 pM for RBD in diluted human serum), a high specificity, a large dynamic range (~ 7 logs), and fast readout within minutes. The rapid detection, low material cost (estimated $< \$0.01$ per test), inexpensive and portable readout system (estimated $< \$5$), and digital data output, make Nano2RED a particularly accessible assay in screening of patient samples towards successful control of infectious diseases.

1. Introduction

In recent times, we have witnessed the emergence of many infectious viral diseases, from the highly fatal Ebola virus disease (EVD, with a fatality rate of 45%–90%) (Couturier et al., 2020; Hoenen et al., 2006) to the highly contagious coronavirus disease 2019 (COVID-19) with its global > 250 million infections and > 5 million deaths as of November 2021 (Worldometer, 2021). Future emergence of Disease X, as contagious as COVID-19 and as lethal as EVD, would pose an even greater threat to humanity, and will be both difficult to prevent or predict. During disease emergence, early pathogen identification and infection

isolation are extremely critical for containing disease transmission (Perkins et al., 2017). Therefore, for effective mitigation, it is necessary to accelerate the design, development, and validation of diagnostic processes, as well as to make the diagnostic tools broadly accessible within weeks of the initial outbreak (Perkins et al., 2017).

Current diagnostic methods rely on the detection of the genetic (or molecular), antigenic, or serological (antibody) markers (Tang et al., 2020). Genetic diagnostics use DNA sequencing, polymerase amplification assays, or most recently, CRISPR technologies (Joung et al., 2020; Kellner et al., 2019). For example, real-time reverse transcription polymerase chain reaction (RT-PCR) tests are viewed as the gold standard

* Corresponding author. School of Electrical, Computer and Energy Engineering, Arizona State University, Tempe, AZ, 85287, USA.

** Corresponding author. Department of Biochemistry, University of Washington, Seattle, WA, 98195, USA.

E-mail addresses: gulc@uw.edu (L. Gu), wangch@asu.edu (C. Wang).

¹ Xiahui Chen, Shoukai Kang and Ashif Iqbal contributed equally to this work.

² Current Address: College of Materials Science and Engineering, Key Laboratory of Advanced Functional Materials, Education Ministry of China, Beijing University of Technology, Beijing 100124, China.

for their high sensitivity; however, these tests are also costly, time-consuming, and instrument-heavy. Genetic tests also can often display false positives by picking up genetic fragments from inactive viruses (Mina et al., 2020). In comparison, antigen and antibody detections are complementary as they allow more rapid, affordable, and accessible detection without complex sample preparation or amplification. As such, these detection methods are viewed as suitable for surveillance and timely isolation of highly infectious individuals, particularly outside clinical settings (Mina et al., 2020). While antibody (e.g., IgM) detection has been used for disease diagnostics (Broadhurst et al., 2016), it is less predictive and more suitable for immune response studies. In comparison, viral protein antigen tests provide a reliable field-test solution in diagnosing symptomatic patients (Albert et al., 2020; Broadhurst et al., 2016; Perkins and Kessel, 2015). In addition, since they are rapid, easy to operate, and low-cost, antigen tests can be deployed at high frequencies and large volumes for in-time surveillance, which is thought to be one crucially important factor in disrupting a virus transmission chain (Larremore et al., 2021; Mina et al., 2020).

Current antigen diagnostics typically employ enzyme-linked immunosorbent assays (ELISA) and lateral flow immunoassays (LFIs). ELISA is the workhorse for analyzing antigens and antibodies, but it requires a multistep workflow and a series of washing steps, hours of incubation prior to readout, and a readout system dependent on substrate conversion and luminescence recording. Deployment of ELISAs in high-throughput mass screenings requires automated liquid handling systems to coordinate the complex workflow, which is not ideal for portable uses. LFIs are potentially much easier to use outside lab settings but usually have much lower sensitivity and thus poorer accuracy compared to ELISA (Lisboa Bastos et al., 2020). Here we report a modular strategy, i.e., nanobody-conjugated nanoparticles for rapid electronic detection (Nano2RED), which can quickly establish a rapid, accessible antigen diagnostic tool within a few weeks of pathogen identification. To generate high-quality affinity reagents within two weeks for any given purified marker protein, we have streamlined a protocol for phage selection of single-domain antibodies (or nanobodies) (Muyldermans 2013) from a highly diverse combinatorial library ($>10^9$). The selected nanobodies were genetically fused with an AviTag for site-specific biotinylation and immobilization onto streptavidin-coated gold nanoparticles (AuNPs), which serve as multivalent antigen binding sensors. Based on only physical signal transduction and readout processes without enzymatic reactions, molecular amplification, fluorescent labeling or chemiluminescence, Nano2RED quantitatively transduces

antigen binding into colorimetric, spectrometric, and electronic readouts (Fig. 1). Uniquely, Nano2RED features portability, low cost, and simplicity while preserving a high sensitivity (LOD of ~ 0.13 pM or 11 pg/mL in Ebola sGP sensing), a high specificity (distinguishing sGP from its membrane-anchored isoform GP1,2) and a large dynamic range (~ 7 logs). Additionally, its electronic readout capability can be extended to automate data collection, storage, and analysis, further reducing the workload health care workers, and speeding up diagnostic and surveillance response.

2. Materials and methods

2.1. Nanobody-binder selection and characterization

sGP and RBD nanobody-binder selection was done according to previously established protocols (Kang et al., 2019). A total of three rounds of biopanning were performed with decreasing amount of antigen (200 nM, 100 nM, 20 nM). Single colonies were picked and validated by phage ELISA followed by DNA sequencing. Identified mono-binders, sGP7, sGP49, RBD8, and RBD10 were expressed as a C-terminal Avi-tagged and His-tagged form in *E. coli*, purified by Ni-affinity and biotinylated by BirA using a BirA-500 kit (Avidity). Their binding kinetics and co-binding activities were measured by Bio-Layer Interferometry (BLI). In order to validate and determine the detection sensitivity of co-binders, a sandwich phage ELISA assay was also performed. More details were provided in supplementary section (Supplementary Section1, 8.4 and 8.5, Tables S1 and S2).

2.2. Nanoparticle functionalization with nanobodies

The streptavidin functionalized gold nanoparticles (for example ~ 0.13 nM 80 nm AuNPs, 80 μ L) were first mixed with an excessive amount of biotinylated nanobodies (about 1.2 μ M, 25 μ L). The mixture was incubated for 2 h, and then purified by centrifuge (accuSpin Micro 17, Thermo Fisher) at 10,000 rpm for 10 min and repeated twice to remove unbound biotinylated nanobodies. The purified AuNP colloid was measured by Nanodrop 2000 from Thermo Fisher to determine the concentration. The concentration of AuNPs was subsequently adjusted to desired optical extinction level (e.g., in our case ~ 0.048 nM for 80 nm AuNPs) and was aliquoted into 12 μ L in Eppendorf tubes.

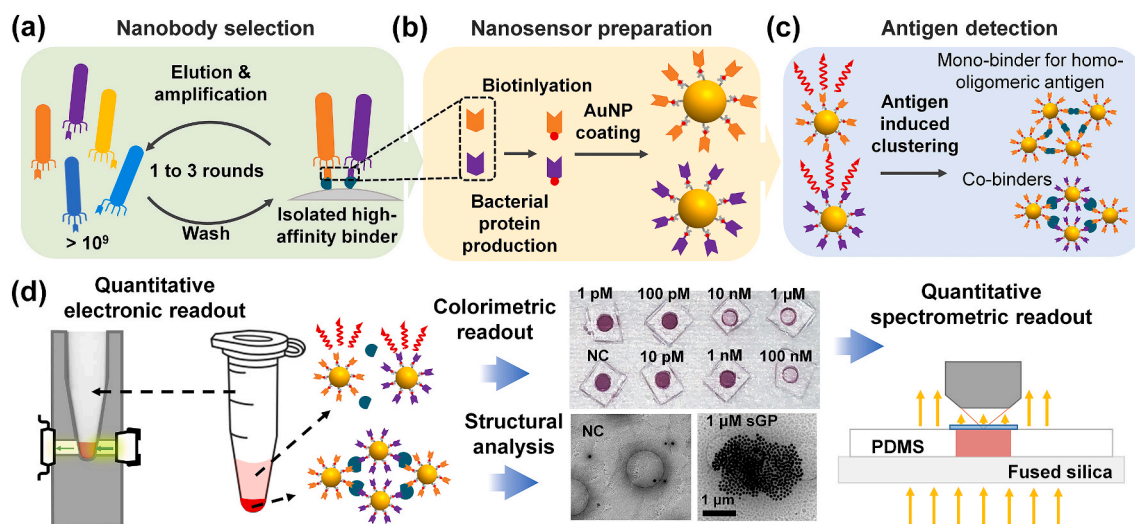


Fig. 1. Overview of Nano2RED assay development and characterizations. (a)–(c) Key steps of nanobody selection and surface function of nanobody on AuNPs. (d) Schematics showing different characterization and readout methods for understanding the assay mechanism, and colorimetric and quantitative determination of antigen concentration.

2.3. Antigen detection

sGP or RBD stock solutions (6 μM , in $1 \times \text{PBS}$) underwent a 10-fold serial dilution to target concentrations (4 pM to 4 μM) in selected detection media. All the buffers contained $1 \times \text{PBS}$, 20% v/v glycerol and 1 wt% BSA, while that volume ratio of FBS (Fetal Bovine Serum), HPS (Human Pooled Serum), and WB (Whole blood) in their corresponding detection media was all 20%. This resulted in a final 5% FBS, HPS, or WB in the detection assay. For example, for sGP detection with co-binders, solutions of sGP49-functionalized AuNPs, sGP7-functionalized AuNP, and sGP were mixed at a ratio of 3:3:2 and thoroughly vortexed. For incubation-based detection, the assay solution was allowed to incubate for ~ 3 h prior to readout. For rapid detection the assay solution was centrifuged (accuSpin Micro 17, Thermo Fisher) at 3,500 rpm (1,200 $\times g$) for 1 min, optionally incubated, and vortexed (mini vortexer, Thermo Fisher) at 800 rpm for 15 s prior to readout. A similar protocol was used for RBD sensing.

2.4. Polydimethylsiloxane (PDMS) well plate fabrication

Sylgard 184 silicone elastomer base was thoroughly mixed with the curing agent (mass ratio 10:1) for 30 min and placed in a vacuum container for 2 h to degas. The mixture was then fully cured at room temperature into a PDMS membrane. The membrane was then cut to desired shape, and 2 mm wells were drilled by punchers. The as-prepared PDMS membrane and a diced fused silica (500 μm thick) were both rinsed with isopropyl alcohol, dried in nitrogen, and treated by oxygen plasma. Immediately after, the two were bonded to form a PDMS well plate. To prevent non-specific bonding of proteins, the PDMS plate was treated with 1 wt% PVA in water solution for 10 min, adapted from previously reported methods (Trantidou et al., 2017). Then, it was dried by nitrogen, heated on a 110 $^{\circ}\text{C}$ hotplate for 15 min, and cooled to room temperature.

2.5. Electronic readout with rapid test

An electronic readout system consists of three key components: a light-emitting diode (LED) light source, a photodiode, and a micro-centrifuge tube holder. The centrifuge tube holder was 3D printed using ABSplus P430 thermoplastic to snugly fit a standard 0.5 mL Eppendorf tube. Holes were opened on the microcentrifuge tube holder to align a LED (597-3311-407NF, Dialight), the upper-level assay liquid, and a photodiode (SFH 2270R, Osram Opto Semiconductors). The LED was powered by two AA batteries (3 V) through a serially connected resistor. The photodiode was reversely biased by three AA batteries (4.5 V) and serially connected to a 7 M Ω load resistor, which converted the photocurrent to voltage output.

2.6. Estimate of limit of detection for Nano2RED

In our work, limit of detection (LOD) was calculated such that the measured signal distinguishes from the reference signal by three times the standard deviation (3σ). For optical and electronic measurement, we used $LoD = c(E_{NC} - 3\sigma)$ and $LoD = c(V_{NC} + 3\sigma)$, respectively. Here E_{NC} and V_{NC} are the extinction intensity and readout voltage for negative control (NC) sample. We compared different methods to estimate σ (Table S1 and Fig. S25), and decided to use pooled sigma from all measurements (σ_{PSA}) for its best consistency. This consistency could be attributed to fact that our data collection is a physical process where the noise is insensitive to reagent concentration. Particularly, when using spectrometric readout, the noise is strongly affected by optical focusing and could happen to any data sets; and therefore the overall average provides a better estimate of the empirical errors. For ELISA measurement, we still used conventional σ_{NC} for LOD determination, given the dependence of noise on reagent concentration.

3. Results and discussion

3.1. Nanobody co-binder selection for AuNP functionalization

We generated nanobody co-binders (*i.e.*, two mono-binders simultaneously binding to non-overlapping epitopes in the same antigen) against target antigens (Fig. 1a) using a fast, robust protocol, including the phage display selection of the combinatorial nanobody library, parallel bacterial protein production, co-binder validation, and AuNP functionalization, that can be completed in less than two weeks upon the availability of an antigen protein (Fig. S1). Nanobodies, a single-domain (12–15 kDa) functional antibody fragments, are ideally suited for low-cost bacterial production (Muyldermans, 2013) towards inexpensive infectious disease detection. To avoid relatively lengthy and costly procedures and animal protection issues associated with traditional antibody screening, we screened the synthetic nanobodies library with an optimized thermostable scaffold prepared in our previous work (Kang et al., 2019). The Ebola antigen, sGP, is a homodimeric isoform of the glycoproteins encoded by a GP gene of all five species of *Ebolavirus* with multiple post-translational modifications (de La Vega et al., 2015). sGP is believed to act as a decoy to disrupt the host immune system by absorbing anti-GP antibodies (de La Vega et al., 2015; Kaushik et al., 2016). Given its abundance in the blood stream upon infection and its quantitative correlation with disease progression and humoral response, sGP is widely used as a circulating biomarker in EBOV diagnostics (Fontes et al., 2021; Kaushik et al., 2016). The chosen SARS-CoV-2 antigen, RBD, engages the viral receptor, human angiotensin-converting enzyme 2 (ACE2), causing conformational changes that trigger a cleavage needed for viral infection (Lan et al., 2020; Wang et al., 2020). It is a major antigenic target for protective antibodies (Wu et al., 2020), and thus is highly significant for diagnostics, as well as for the development of vaccines and therapeutic neutralizing antibodies (Hotez et al., 2020; Robbiani et al., 2020).

To efficiently identify nanobodies that can bind non-overlapping epitopes of an antigen protein, we assessed clonal diversity and co-binding abilities of candidates enriched in different biopanning rounds (Fig. 2a). The two top co-binder pairs, termed sGP7–sGP49 and RBD8–RBD10, were bacterially expressed and purified (Fig. 2b) with high yields (1.5–6 mg per liter of culture). Their equilibrium dissociation constants (K_D) were measured to be in the nanomolar range by Bio-Layer Interferometry (BLI) (Fig. 2c) and the co-binding activities were validated by ELISA (Fig. 2d and Fig. S1b) and BLI (Fig. 2e and Fig. S1b). Lastly, nanobodies were biotinylated with *E. coli* biotin ligase (BirA) as previously reported (Kang et al., 2019) and then loaded to streptavidin-coated AuNPs (see Methods section and Supplementary information).

3.2. Nanobody-functionalized nanoparticles for sensing

In our assay design, AuNPs densely coated with biotinylated nanobodies allow multivalent antigen sensing (Fig. 1a and b) known to significantly enhance antigen binding compared to the monovalent binding (Greenspan and Cooper, 1993; Hornick and Karush, 1972). Further, the multivalent binding also facilitates AuNP aggregation and subsequent precipitation, producing antigen-concentration-dependent signals within minutes. In our proposed sensing scheme (Fig. 1b), AuNPs, without observed nonspecific particle-particle interaction, are initially homogeneously dispersed in colloid, presenting a reddish color from localized surface plasmon resonance (LSPR) extinction (Eustis and El-Sayed, 2006). Upon mixing with viral antigens, multiple AuNPs are pulled together by the antigen-nanobody binding to gradually form aggregates. The formation of AuNP aggregates gradually broadens LSPR extinction as simulated by finite-difference time-domain (FDTD) method (Supplementary section 2 and Fig. S2), and form pellets as gravity overtakes the fluidic drag force (Fig. 1c-d). This leads to increased transparency of the AuNP colloid, which were precisely described in

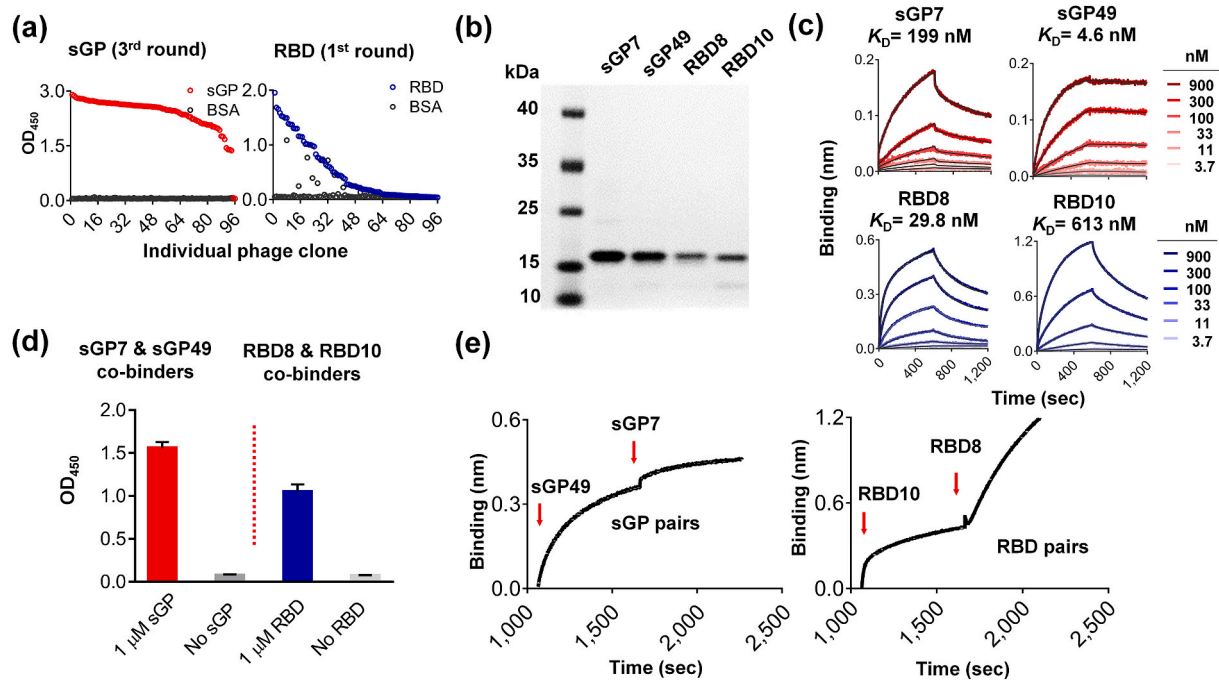


Fig. 2. Identification and characterization of antigen-specific nanobody binders. (a) Binding of single phage clones to antigen measured by ELISA. Biotinylated sGP (red) and RBD (blue) were immobilized on streptavidin-coated plates, respectively. BSA was used as a control. (b) SDS-PAGE analysis of purified sGP and RBD-specific binders. (c) BLI analysis of specific binders binding to sGP (upper: red lines) and RBD (lower: blue lines) at different concentrations. The sGP and RBD were immobilized on streptavidin biosensors (SA). Measured data were globally fitted (grey lines). (d) Co-binder validation by sandwich ELISA. The first biotinylated nanobody binders (sGP49 and RBD10) were immobilized on a plate, incubated with or without antigen, and then the second binders (sGP7 and RBD8) were detected by a horseradish peroxidase-conjugated antibody. (e) Co-binder validation by two-step binding characterization using BLI. Biotinylated sGP (top panel) and RBD (bottom panel) were immobilized on SA sensors. Epitope binning was performed by first dipping into the first binder well for 750 s for saturation and then incubation with second binder.

DNA and protein sensing (Mirkin et al., 1996; Thanh and Rosenzweig, 2002). The color change is further quantified by us in a well plate by spectrophotometer or using a simple electronic device.

3.3. Colorimetric and spectrometric sensing of sGP

The size and shape of AuNPs determine the optical extinction and the suspension color, hence affecting the sensitivity and assay incubation time (Figs. S3 and S4). Here, the AuNP size effect was studied with NP diameters of 40, 60, 80, and 100 nm in sensing of Ebola sGP proteins using sGP49 nanobody in 1 \times PBS buffer (Supplementary section 3). To standardize the measurement, a UV-visible spectrometer (Fig. S3a) was used to inspect sGP sensing samples (5 μ L), which were collected from top-level liquid in microcentrifuge tubes, in custom-designed PDMS well plate (Fig. S3b). Clearly (Fig. S4 a-d), the color of the assay is redder for small NPs but greener for larger ones, attributed to a redshift in extinction resonance wavelengths at larger NP sizes. Additionally, a significant color contrast was observed in distinguishing 10 nM and higher sGP concentration from the reference negative control (NC) sample (with only PBS buffer but no sGP) for all AuNP sizes, indicating that sGP can be readily detected by the naked eye.

The impact of AuNP size on sGP detection was further studied (Fig. S4e-l) by measuring the AuNP extinction, which is correlated with its concentration $[NP]$ and diameter d following $\sigma_{ext} \propto [NP]d^3$ (Link and El-Sayed, 1999). A decrease in extinction indicated a drop in $[NP]$ in the upper-level solution caused by antigen-induced AuNP precipitation, evidenced by plotting the AuNP extinction peak values as standard curves against the sGP concentration at each AuNP size (Fig. S4i-l). This incubation-based assay had a dynamic range of \sim 100 pM to \sim 100 nM for all AuNP sizes. The incubation was found to take 4–7 h, using 10 nM sGP in 1 \times PBS as the test molecule (Fig. S4m-p). From these experimental analyses, we chose 80 nm AuNPs to further characterize the

assay performance in sGP sensing (Fig. 3a). This selection was based on several factors: their slightly higher sensitivity (\sim 15 pM, compared to \sim 100 pM for other sizes), larger detection dynamic range (up to 4 logs, compared to 2 to 3 logs for other sizes), and shorter incubation time (3–4 h, compared to 4–7 h for other sizes).

To understand the assay's working mechanism, we complemented the solution-phase optical testing by inspecting the AuNP precipitates in solid state using different structural and optical characterization methods (Supplementary section 4). First, cryogenic transmission electron microscope (CryoTEM) images showed aggregates of AuNPs formed with 1 nM sGP (Fig. 3a), while only AuNPs but not clusters were observed in the upper-level liquid (Fig. 3b) or in the precipitates of the NC sample (Fig. S5). This proved that AuNP precipitation serves to transduce antigen binding to solution color change for sensing readout (Fig. 1). Further, we have performed drop-casting to deposit AuNP upper-level liquid samples on glass slides for optical extinction analysis (Figs. S6 and S7) and on gold films for scanning electron microscopy (SEM) and dark field scattering imaging (Figs. S8, S9, and S10). The measurement results were, in general, consistent with spectrometric in-solution sGP detection using PDMS well plate, but inferior in sensitivity (150 pM for SEM, \sim 174 pM for drop-cast on glass slide, and \sim 1 nM for dark filed imaging, Table 1). The decreased sensitivity could be attributed to inherent variations associated with sample preparation and background noise in the readout systems.

sGP was further detected in diluted fetal bovine serum (FBS, 5%) using 80 nm sGP49-functionalized AuNPs (Fig. 3c-h). Similarly, after 3-h incubation in microcentrifuge tubes (Fig. 3c), the upper-level liquid samples were loaded into a PDMS well plate (Fig. 3d) and measured by spectrometer (Fig. 3e). Plotting extinction peak values against sGP concentration (Fig. 3f), we noticed our assay could again detect sGP from 10 pM to 100 nM, which supports clinically relevant Ebola detection from patients' blood (sub-nM to μ M) (Escudero-Pérez et al.,

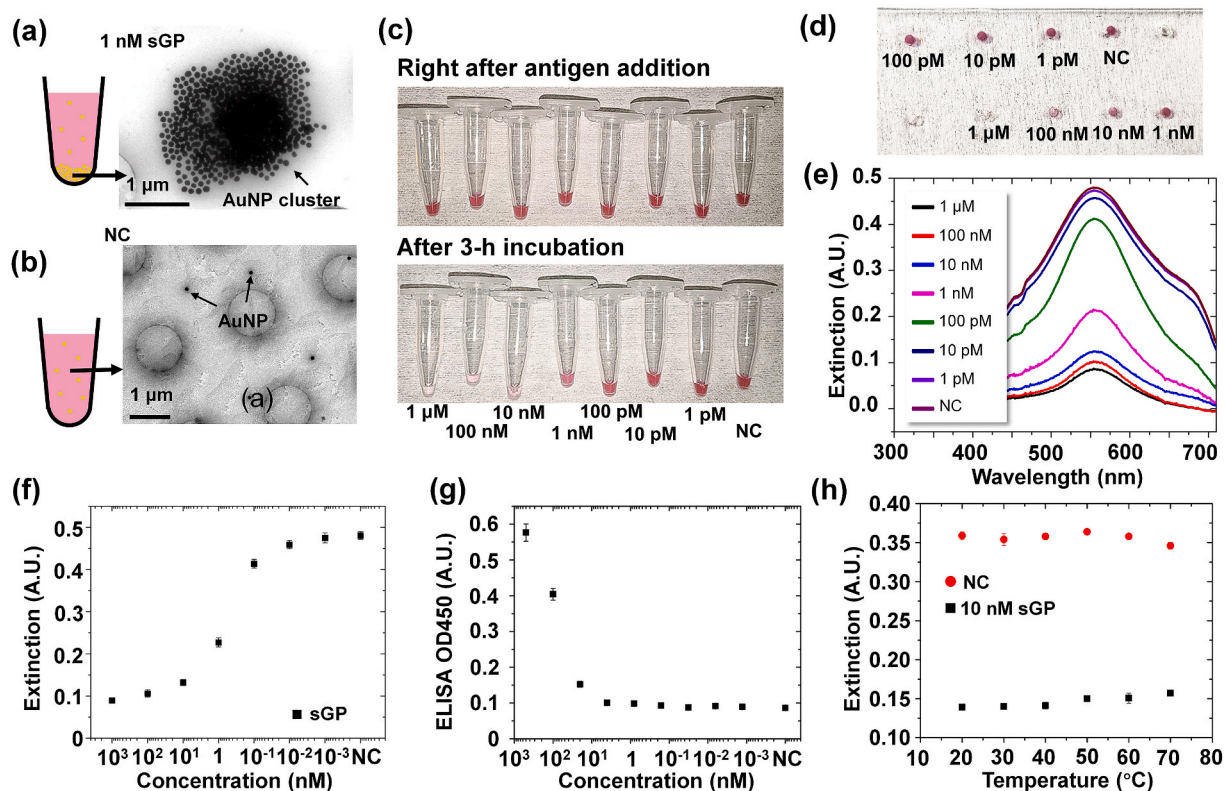


Fig. 3. Ebola sGP sensing using mono-binder antibody sGP49 by incubation. (a–b) Cryo-TEM image of precipitates after 3-h incubation: (a) with 1 nM sGP, (b) the negative control (NC) sample (no sGP). (c) Visual images of samples loaded in microcentrifuge tubes, right after mixing and 3 h after incubation. (d) The upper-level liquid samples loaded in PDMS well plate. (e) Extinction spectra measured from PDMS well plate. (f) Extinction peak (559 nm) values plotted against sGP and GP1,2 concentrations. (g) Optical signals (optical density at 450 nm) measured by sandwich ELISA in detection of sGP. (h) Extinction peak (559 nm) values extracted from spectroscopic measurements in detecting 10 nM sGP and NC at temperatures from 20 °C to 70 °C. The buffer was $1 \times$ PBS in Figures a and b, and 5% FBS in Figures c to h. The sGP concentration was from 1 pM to 1 μ M. NC sample was the buffer without sGP or GP1,2. The AuNPs were 80 nm in all measurements.

2014; Sanchez et al., 1996). Here the three-sigma (3σ) LoD, or $E_{NC} - 3\sigma$ (see methods section), was found to be about 15 pM (or 1.25 ng/mL), in comparison to that measured using sGP49 phage ELISA (LOD \sim 80 pM, Fig. 3g and Supplementary Table S1). The LOD can be understood from estimations based on the nature of multivalent antigen binding (supplementary section 5). We also found the 10 nM sGP could be easily distinguished from NC sample at a broad temperature range from 20 to 70 °C (Fig. 3h). This indicates our assay is stable at ambient temperatures without serious concerns of performance degradation during transportation or storage, which is very important for mass screening.

3.4. Rapid antigen detection

The 3-h incubation was useful for effective AuNP bridging and precipitation, and still shorter than ELISA and much better than many RT-PCR assays. However, rapid diagnostics, that is, less than 30 min, is more desirable for accessible infectious disease diagnosis and control of disease spread. Here, we further studied the rate-limiting sensing mechanism to reduce the detection time (Supplementary section 6.1). In conventional ELISA assays, the antigen diffusion process is usually the rate-limiting step (Stenberg and Nygren, 1988), given long diffusion length (millimeter scale liquid depth) and slow fluidic flow speed at plate surfaces, and leads to a long assay time. Differently, the use of NPs as reaction sites significantly decreases the diffusion length to about 1 μ m at a high NP concentration (e.g. experimentally \sim 0.036 nM for 80 nm AuNPs). Additionally, the small size and mass of AuNPs (5×10^{-15} g) result in a high diffusivity ($D_{NP} \sim 4.2 \mu\text{m}^2/\text{s}$ from Stokes–Einstein equation) and a high thermal velocity (estimated 0.028 m/s), further promoting effective fluidic transport and antigen binding, with an estimated diffusion time of <1 s.

We further investigated the physical processes of AuNP aggregation and precipitation. Here, using a simplified model based on Smoluchowski's coagulation equation (Fig. 4a–b, and more details in Supplementary section 6.2) (Deaconu and Tanré, 2000), we determined that an empirical parameter P , which defines the probability of antigen-nanobody binding per collision, was ~ 1 in the model to best fit experimental data. This indicated very high-affinity binding, and suggested that the multivalence of the nanobody-bound AuNPs greatly improves the observed “functional affinity” compared to intrinsic mono-binding affinity (Greenspan and Cooper, 1993; Hornick and Karush, 1972). Interestingly the ELISA-measured binding kinetics, which essentially measured mono-binding affinity, failed to depict the observed nanobody-antigen binding in solution (Piehler and Schreiber, 1999; Rich et al., 2008). Additionally, our model estimated τ_{agg} as ~ 0.87 h at 0.036 nM AuNP in detection of 10 nM sGP, but also predicted that τ_{agg} could be greatly reduced, for example to 0.024 h or 36 times shorter when using 50 times more concentrated NPs. On the other hand, the sedimentation time can be estimated using the Mason-Weaver equation by $\tau_{sed} = z/(s \cdot g)$, where z is the precipitation path (for example the height of colloid liquid), g is the gravitation constant, and s is the sedimentation coefficient dependent on the physical properties of AuNPs and buffers (Midelet et al., 2017). Given that $z \sim 3.5$ mm for 16 μ L liquid in a microcentrifuge tube, we calculated that τ_{sed} decreases from 26 h for 80 nm AuNPs to 1.0 and 0.3 h for a 400 nm and 800 nm diameter cluster (comparable to experimentally observed clusters in micrometer size at 1 nM sGP, Fig. S5), respectively.

For rapid detection, we introduced a centrifugation step (1,200 \times g, 1 min) after antigen mixing to both enhance the reagents' concentration and decrease the precipitation path (Fig. 4c, additional data in Supplementary section 7). This step concentrated AuNPs at the bottom of

Table 1
Performance of the Nano2RED

Ebola sGP protein sensing										
Assay format	Readout method	Readout system	Readout system cost	Readout system size	Assay time	Nano-body	Buffer	Diagnostic sensitivity		
								pM	pg/mL	
Incubation	Spectrometric	Lab microscope	~\$25,000	~3 m ³	3-4 h	sGP49	FBS	15	1250	
	Spectrometric (cast on glass)	Lab microscope	~\$25,000	~3 m ³	3-4 h	sGP49	PBS	174	14529	
Centrifuge-accelerated (rapid)	Dark Field (cast on gold)	Lab microscope	~\$25,000	~3 m ³	3-4 h	sGP49	PBS	1000	83500	
	SEM (cast on gold)	SEM	~\$65,000	3-5 m ³	3-4 h	sGP49	PBS	150	12530	
	Colorimetric	Eyes or smart phones	~\$200 (phone)	~78 cm ³	5-20 min	sGP49	FBS	1000	83500	
	Colorimetric	Eyes or smart phones	~\$200 (phone)	~78 cm ³	5-20 min	sGP7/ sGP49	FBS	100	8350	
	Colorimetric	Eyes or smart phones	~\$200 (phone)	~78 cm ³	5-20 min	sGP49	FBS	80	6680	
	Colorimetric	Eyes or smart phones	~\$200 (phone)	~78 cm ³	5-20 min	sGP7/ sGP49	PBS	0.16	13	
	Spectrometric	Lab microscope	~\$25,000	~3 m ³	5-20 min	sGP7/ sGP49	FBS	1.05	88	
	Spectrometric	Lab microscope	~\$25,000	~3 m ³	5-20 min	sGP7/ sGP49	HPS	1.26	105	
	Spectrometric	Lab microscope	~\$25,000	~3 m ³	5-20 min	sGP7/ sGP49	WB	18.2	1520	
	Spectrometric	Portable spectrometer	~\$1,000	~170 cm ³	5-20 min	sGP49	FBS	99	8270	
SARS-CoV-2 RBD protein sensing	Assay format	Readout method	Readout system	Readout system cost	Readout system size	Assay time	Nano-body	Buffer	Diagnostic sensitivity	
									pM	pg/mL
Centrifuge-accelerated (rapid)	Colorimetric	Eyes or smart phones	~\$200 (phone)	~78 cm ³	5-20 min	RBD8/ RBD10	FBS	1000	29180	
	Spectrometric	Lab microscope	~\$25,000	~3 m ³	5-20 min	RBD8/ RBD10	PBS	1.4	42	
	Spectrometric	Lab microscope	~\$25,000	~3 m ³	5-20 min	RBD8/ RBD10	FBS	5.23	153	
	Spectrometric	Lab microscope	~\$25,000	~3 m ³	5-20 min	RBD8/ RBD10	HPS	22.3	649	
	Spectrometric	Lab microscope	~\$25,000	~3 m ³	5-20 min	RBD8/ RBD10	WB	253.3	7372	
	Electronic	LED & photodetector	~\$5	~4 cm ³	5-20 min	RBD8/ RBD10	HPS	1.35	39	

microcentrifugation tubes without causing non-irreversible AuNP aggregation, with an estimated z of $\sim 150 \mu\text{m}$ from optical image (Fig. 4d), i.e. a roughly >20 times reduction in z and accordingly τ_{sed} . Additionally, the concentrated AuNPs are confined to an estimated $<0.34 \mu\text{L}$ volume, or ~ 50 times concentration increase from original $16 \mu\text{L}$ colloid liquid, leading to a greatly reduced τ_{agg} , estimated from 0.87 h to 0.024 h (Fig. 4b). These calculations indicate that both the aggregate formation and precipitation can take place in just a few minutes. Experimentally, the assay colloid was incubated for 20 min after centrifugation and then thoroughly vortexed, which served to re-suspend free AuNPs at the tube bottom. Indeed, the increased upper-level assay liquid transparency at higher sGP concentration (Fig. 4e) was distinguished visually for sGP $>1 \text{ nM}$. The extinction values of the upper-level liquid (Fig. 4f) at its peak wavelength ($\sim 559 \text{ nm}$) (Fig. 4g) were plotted against sGP concentration along with the 3-h incubation results, showing comparable performance in dynamic range and LOD ($\sim 80 \text{ pM}$). Using 10 nM sGP as the antigen, we found the color contrast was high enough to be immediately resolved by the naked eye after vortex mixing, requiring minimal incubation (Fig. 4h and S11a). Including all of the operation steps for sample collection, pipetting, centrifugation, vortex mixing, and readout, this rapid test scheme can be completed in a few minutes.

3.5. Rapid sGP detection with a portable, electronic readout device (Nano2RED)

To further simplify diagnostics without bulky spectrometer or microscopy systems, we demonstrated the feasibility of detecting sGP in FBS using a cost-efficient, portable UV-visible spectrometer system for field deployment (Fig. S13). Additionally, we developed a homemade electronic readout system with significantly reduced system cost to deliver accurate and sensitive detection results comparable to a lab-based spectrometer system (Fig. 4i-k). Here, an LED light source emitted narrowband light at the AuNP extinction peak ($\lambda_p = 560 \text{ nm}$, $\text{FWHM}_p = 40 \text{ nm}$), which transmitted through the upper-level assay liquid and then was collected by a photodiode (Fig. 4i). As a result, a photocurrent or photovoltage was generated on a serially connected load resistor in a simple circuitry that can be easily integrated and scalably produced. In practice, we 3D-printed a black holder to snug-fit a microcentrifuge tube, and mounted the LED and photodetector on the holder (Fig. 4j). The LED and photodiode bias voltages were set to ensure wide-range detection of sGP proteins without saturating the photodetectors. Using 80 nM sGP49-functionalized AuNP Nano2RED assays, sGP was detected in diluted FBS (5%) with a handheld multimeter (Fig. 4k, V_R , in blue triangle and dashed line). Compared to lab-based spectrometric readout (in black square and solid line), the

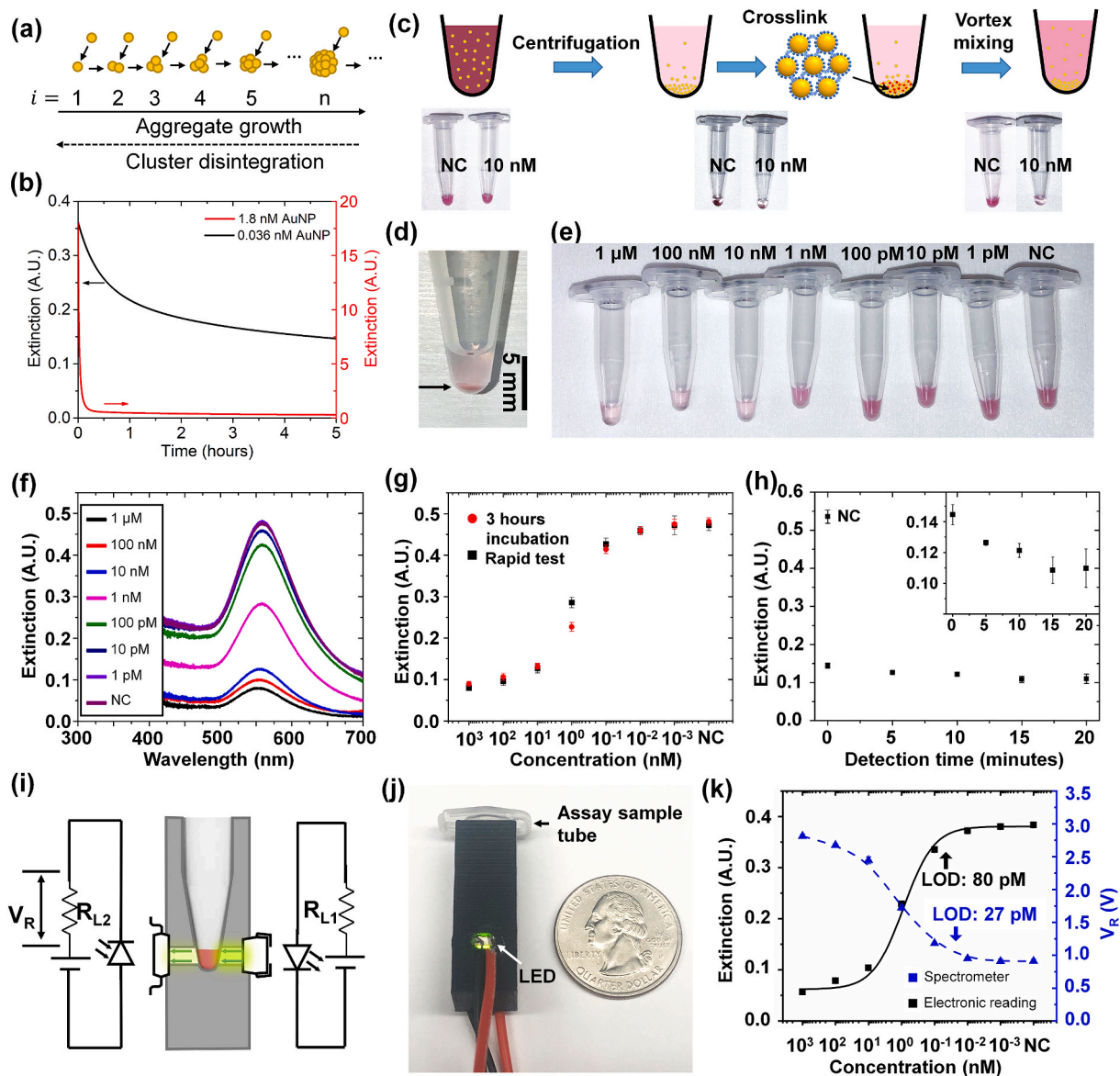


Fig. 4. Rapid and electronic detection of sGP using mono-binder antibody sGP49 with improved sensing performance. (a) Modeling of aggregate formation by considering only AuNP monomer-oligomer interactions. (b) Time-dependent extinction calculated for 0.036 nM (black, as used in our experiments) and 1.8 nM (red, 50 × concentrated) 80 nm AuNPs in detecting 10 nM sGP. (c) Schematic showing key steps in rapid detection protocol: centrifugation, AuNP aggregation through incubation, and vortex-mixing. (d) Visual image of AuNPs (80 nm, concentration 0.036 nM) after centrifugation at 3,500 rpm for 1 min. (e) AuNPs in microcentrifuge tubes for rapid detection of 1 pM to 1 μM sGP in 5% FBS. The tubes were centrifuged at 3,500 rpm for 1 min and vortex-mixed for 15 s. (f) Extinction spectra of AuNPs shown in (e). (g) Extinction peak values (559 nm) extracted from (f) and plotted against sGP concentration in rapid detection. Measurement results of incubation-based tests were plotted in red for comparison. (h) Effect of incubation time on the extinction measured for samples in detecting 10 nM sGP in 1 × PBS. Inset shows narrowed extinction range for visual contrast. (i–k) Electronic detection of sGP in 5% FBS using miniaturized measurement system: (i) Schematic and (j) Visual image of electronic readout system, consisting mainly of a LED circuit, a photodiode circuit, and a 3D printed Eppendorf tube holder. (k) Voltage signals measured in detecting sGP in 5% FBS, shown as Blue Triangle and dashed line. Lab-based spectrometer-measured extinctions of the same assays are plotted in Black Square and solid line.

electronic readout displayed identical dynamic range but improved LOD (27 pM compared to 80 pM).

3.6. Detection of sGP and RBD in serum and blood

We further evaluated the use of co-binding nanobodies in sGP and RBD sensing (Figs. 5 and S28), *i.e.*, sGP49/sGP7 for sGP and RBD8/RBD10 for RBD (Fig. 2), and performed rapid detection in PBS, FBS, human pooled serum (HPS), and whole blood (WB) (additional data in Supplementary section 8 and Figs. S15–S23). The incubation and rapid assay formats with the assay performance, instrument costs, and LODs were summarized in Table 1, and additional data on measurement

variance (sigma) and LOD were summarized in Supplementary Tables S1 and S2. There are several notable observations. First, using sGP sensing as an example and comparing to previously reported results (Fontes et al., 2021; Zang et al., 2019) (Supplementary Table S2), Nano2RED consistently produced ~130 fM to 1.3 pM LOD (or ~10–100 pg/mL) in PBS, FBS, and HPS with spectrometric and electronic readout. It is noted very recently co-binder-based D4 assay format reported ~30 pg/mL LOD in human serum, and was able to detect the Ebola virus earlier than PCR in a monkey model (Fontes et al., 2021). In LOD comparison, our Nano2RED (~10 pg/mL with electronic readout) was even better, indicating its competitiveness in high-precision diagnostics.

Additionally, our study (Table 1) also revealed the importance of a systematic assay design strategy, from molecular binding to signal transduction and readout, to optimize antigen detection. It is clear that the co-binder pair improved the LOD by 10–100 times compared to the mono-binder (sGP49, k_D 4.6 nM), despite a relatively low k_D of 199 nM for the second binder (sGP7) (Fig. 2). This improved sensitivity is likely because the co-binders have a favorable, non-competitive binding configuration that serves to improve antigen binding and AuNP aggregation. Uniquely, the use of a portable and inexpensive electronic readout did not negatively affect the LOD of Nano2RED, but rather improved it compared to spectrometric readout (Fig. 5b and 5g, and Table 1). This can be attributed to smaller 3- σ errors in the electronic readout (Supplementary Table S2), partly due to minimized signal fluctuation by reducing manual operation compared to optical imaging. In addition, the use of biological buffers could also affect detection. For both Ebola sGP and SARS-CoV-2 RBD, the LOD was about 5–10 times worse in serum (FBS and HPS) than in PBS, and further increased by another 10 times in WB. Noticeably, colorimetric readout became challenging in WB sample due to background color interference, but the spectrometric or electronic readout could still readily identify the sGP or RBD extinction signals from the background WB absorption for accurate detection (Fig. S19e and Fig. 5b for sGP and Fig. S25e and Fig. 5h for RBD), indicating the feasibility of Nano2RED for field use with minimized sample preparation.

Fundamentally different from conventional high-sensitivity antigen diagnostics that usually require bulky and expensive readout systems, as well as long assay time, Nano2RED is an affordable and accessible diagnostic technology. For example, sGP sensing using NP-enhanced fluorescent readout would require hours of image processing for optimal sensing with reduced noise (Zang et al., 2019), and these fluorescent systems usually require cubic-meter space and cost \$40,000 or

more (a high-end fluorescent camera costs ~\$25,000). Similarly, a D4 co-binder assay requires a lab-based fluorescent system and ~60 min assay time to achieve PCR-comparable diagnostic sensitivity (Fontes et al., 2021). Its sensitivity drops ~10 times to 100 pg/mL when using a customized fluorescent system, which still costs ~\$1,000 and occupies ~3,000 cm³. The performance further decreases to 6,000 pg/mL when using LFA with colorimetric readout (Fontes et al., 2021). Clearly standing apart, Nano2RED utilizes miniaturized and low-cost semiconductor devices for signal readout with a very small footprint (4 cm³ for tube holder, or <100 cm³ for the whole system, including batteries and meters, which all could be miniaturized on a compact circuit board in the future). The readout system is very low-cost (LED and photodiode each <\$1 here, but can be <\$0.1 when used at large scale, with the total system cost estimated well below \$5), and offers a rapid readout (5–20 min, depending on incubation time after centrifugation). Further, the electronic readout is more accurate than the colorimetric readout, more accessible, without color vision limitations, and more readily available for data storage in computers or online databases for real-time or retrospective data analysis. Additionally, we have estimated the reagent cost in Nano2RED is only about \$0.01 per test (Supplementary section 9), since it requires only a small volume (~20 μ L) of reagents.

We tested sGP against GP1,2, a homotrimer glycoprotein transcribed from the same GP gene and sharing its first 295 residues with sGP (de La Vega et al., 2015), both in FBS (Fig. 5d and S28). The close relevance of GP1,2 to sGP makes it a very strong control molecule to assess our assay's specificity. Indeed, GP1,2 did not produce detectable signals unless higher than 1 nM, indicating a high selectivity over a broad concentration range (100 fM to 1 nM, or 4 logs) where minimal nanobody binding or AuNP aggregation occurred. We also confirmed the weak cross reaction between the sGP binders and GP1,2 by ELISA (Fig. S1c). A high assay specificity is crucial for minimizing false positive diagnosis of

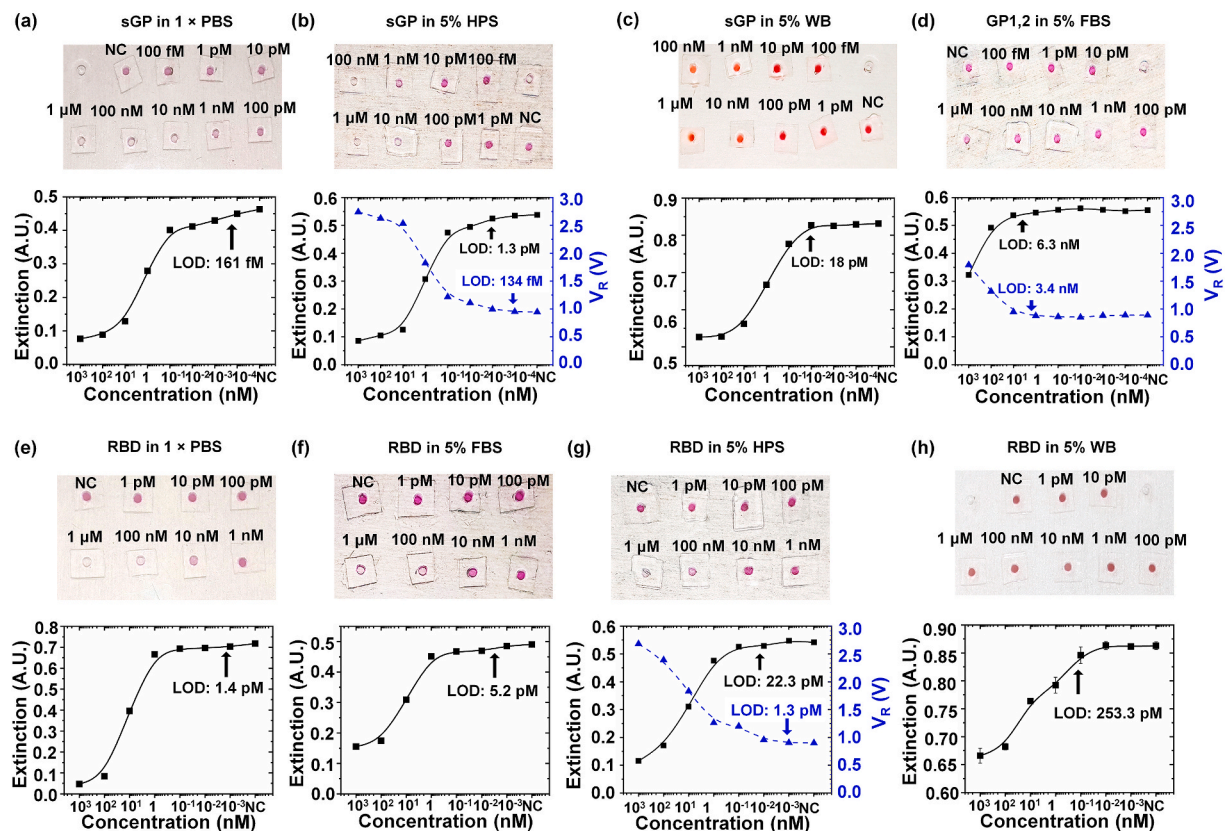


Fig. 5. Co-binders for rapid sGP and RBD detection in different buffers. (a–c) sGP test in 1X PBS, 5% HPS, and 5% WB. (d) GP1,2 as a control sample in 5% FBS. (e–h) RBD test in 1X PBS, 5% FBS, 5% HPS, and 5% WB. Top panels: Optical images of PDMS well plates after rapid test. Bottom panels: Optical sensing (extracted extinction peak values, in black squares, connected with solid lines) and electronic sensing (readout voltage, in blue triangles, connected with dash-lines).

infectious diseases, which could lead to unnecessary hospitalizations and even infections. Considering that 10 nM and higher sGP concentration is typical for EVD patients (Escudero-Pérez et al., 2014; Sanchez et al., 1996; Shubham et al., 2018), Nano2RED is particularly suitable for high-speed mass screening of EVD susceptible populations. Further, SARS-CoV-2 RBD proteins were also detected in the single-digit picomolar range in PBS, FBS, and HPS, with the best LOD (Table 1, 1.3 pM, or ~40 pg/mL, Fig. S1d) again achieved with electronic readout. The LOD in RBD sensing is ~10 times higher compared to sGP sensing, mainly attributed to lower binding affinities of the nanobodies obtained from a single-round biopanning (Fig. 2). Tighter binders can be selected using more biopanning rounds; however, the detection of RBD, a monomeric protein target, serves to demonstrate the general feasibility of the Nano2RED co-binding assay in detection of a broad range of antigens, regardless of their complex molecular structures. Considering the fact that the spike protein is a trimer and each SARS-CoV-2 particle is covered with ~20 copies of such trimers (Ke et al., 2020), the detection of SARS-CoV-2 virus particles could behave differently.

4. Conclusions and outlook

We have demonstrated a generalizable and rapid assay design and pipeline that combines fast affinity reagent selection and production with nanometer-scale theoretical analysis and experimental characterization for optimized sensing performance. Synthetic, high-affinity, co-binding nanobodies could be quickly produced by a phage display selection method from a premade combinatorial library for any given antigen, and proved to be effective in detecting dimeric Ebola sGP and monomeric SARS-CoV-2 RBD proteins. The Nano2RED utilized unique signal transduction pathways to convert biological binding into electronic readout. Using simple electronic circuitry, it starts with AuNP aggregation, which triggers AuNP cluster sedimentation, and then enables AuNP-concentration-dependent optical extinction. Nano2RED eliminates the need for long-time incubation in conventional ELISA and other plane surface-based assays, as well as its associated cumbersome washing steps. The introduction of brief centrifugation and vortex mixing further greatly shortens the aggregation and sedimentation time, enabling rapid tests (within 5–20 min) without sacrificing sensitivity or specificity. Nano2RED is highly sensitive (sub-picomolar or ~10 pg/mL level for sGP) and specific in biological buffers while also affordable and accessible. The demonstrated broadband dynamic range (~100 fM to 1 μM for co-binders, or 7 logs), high sensitivity, high specificity, and broad applications therefore make our Nano2RED assay highly feasible for precise antigen quantification and detection of early-stage infection. It can also be used for high-frequency at-home or in-clinic diagnostics, as well as in resource-limited regions, which could greatly enhance control of disease transmission. The digital data format will in future reduce human intervention in data compiling and reporting, while facilitating fast and accessible data analysis. Nano2RED may find immediate use in the current COVID-19 pandemic for both antigen and antibody detection, as well as preparing for future unforeseeable new outbreaks.

CRedit authorship contribution statement

Xiahui Chen: Methodology, Validation, Formal analysis, Writing – original draft. **Shoukai Kang:** Methodology, Validation, Formal analysis, Writing – review & editing. **Ashif Ikbal:** Investigation, Validation, Formal analysis, Writing – review & editing. **Zhi Zhao:** Investigation. **Yuxin Pan:** Investigation. **Jiawei Zuo:** Investigation. **Liangcai Gu:** Conceptualization, Methodology, Supervision, Review & editing, Project administration, Funding acquisition. **Chao Wang:** Conceptualization, Methodology, Formal analysis, Supervision, Writing – original draft, Review & editing, Project administration, Funding acquisition, Resources.

Declaration of competing interest

The authors declare the following financial interests/personal relationships which may be considered as potential competing interests: Patents on the assay design have been filed by the authors (U.S. Patent Application No. 17/489,273; International Application No. PCT/US2021/052692).

Acknowledgements

This work was supported by a grant from the U.S. National Institutes of Health (1R35GM128918) to L. Gu., C. Wang, X. Chen, M.A. Ikbal and J. Zuo acknowledge partial support from National Science Foundation (NSF) under grant no. 1809997, 1847324, and 2020464. The samples were characterized in the Nanofab cleanroom and Eyring Materials Center (EMC) at Arizona State University. Access to the EMC was supported, in part, by NSF grant no. 1542160. We thank Y. Yao for the use of the portable spectrometer system, M. Goryll for constructive discussion on electronic readout system, B. Ipema and S. Myhajlenko for support in electronic measurement setup, D. Baker and L. Stewart for providing recombinant sGP and GP1,2 proteins, Y. Liang for the help on sGP biopanning, D. Williams for cryoTEM inspections, and S. Vittal and T. Christenson for help on editing the manuscripts.

Appendix A. Supplementary data

Supplementary data to this article can be found online at <https://doi.org/10.1016/j.bios.2022.113971>.

References

- Albert, Eliseo, Torres, Ignacio, Bueno, Felipe, Huntley, Dixie, Molla, Estefanía, Fernández-Fuentes, Miguel Ángel, Martínez, Mireia, Poujois, Sandrine, Forqué, Lorena, Valdivia, Arantxa, de la Asunción, Carlos Solano, Ferrer, Josep, Colomina, Javier, Navarro, David, 2021. Field evaluation of a rapid antigen test (Panbio™ COVID-19 Ag Rapid Test Device) for COVID-19 diagnosis in primary healthcare centres. *Clin. Microbiol. Infect.* 27 (3), 472.e7–472.e10.
- Broadhurst, M.J., Brooks, T.J.G., Pollock, N.R., 2016. *Clin. Microbiol. Rev.* 29 (4), 773–793.
- Couturier, C., Wada, A., Louis, K., Mistretta, M., Beitz, B., Povogui, M., Ripaux, M., Mignon, C., Werle, B., Lugari, A., Pannetier, D., Godard, S., Bocquin, A., Mely, S., Béavogui, I., Hébelamou, J., Leuenberger, D., Leissner, P., Yamamoto, T., Lécine, P., Védrine, C., Chaix, J., 2020. *PLoS Neglected Trop. Dis.* 14 (1), e0007965.
- de La Vega, M.-A., Wong, G., Kobinger, G.P., Qiu, X., 2015. *Viral Immunol.* 28 (1), 3–9.
- Deaconu, M., Tanré, E., 2000. *Ann. della Scuola Norm. Super. Pisa - Cl. Sci.* 29 (3), 549–579.
- Escudero-Pérez, B., Volchkova, V.A., Dolnik, O., Lawrence, P., Volchkov, V.E., 2014. *PLoS Pathog.* 10 (11), e1004509.
- Eustis, S., El-Sayed, M.A., 2006. *Chem. Soc. Rev.* 35 (3), 209–217.
- Fontes, C.M., Lipes, B.D., Liu, J., Agans, K.N., Yan, A., Shi, P., Cruz, D.F., Kelly, G., Luginbuhl, K.M., Joh, D.Y., 2021. *Sci. Transl. Med.* 13 (588), eabd9696.
- Greenspan, N.S., Cooper, L.J., 1993. Cooperative Binding by Mouse IgG3 Antibodies: Implications for Functional Affinity, Effector Function, and Isotype Restriction. *Springer seminars in immunopathology*, pp. 275–291. Springer.
- Hoenen, T., Groseth, A., Falzarano, D., Feldmann, H., 2006. *Trends Mol. Med.* 12 (5), 206–215.
- Hornick, C.L., Karush, F., 1972. *Immunochemistry* 9 (3), 325–340.
- Hotez, P.J., Corry, D.B., Bottazzi, M.E., 2020. *Nat. Rev. Immunol.* 20 (6), 347–348.
- Joung, J., Ladha, A., Saito, M., Kim, N.-G., Woolley, A.E., Segel, M., Barretto, R.P.J., Ranu, A., Macrae, R.K., Faure, G., Ioannidi, E.I., Krajcski, R.N., Bruneau, R., Huang, M.-L.W., Yu, X.G., Li, J.Z., Walker, B.D., Hung, D.T., Greninger, A.L., Jerome, K.R., Gootenberg, J.S., Abudayyeh, O.O., Zhang, F., 2020. *N. Engl. J. Med.* 383 (15), 1492–1494.
- Kang, S., Davidsen, K., Gomez-Castillo, L., Jiang, H., Fu, X., Li, Z., Liang, Y., Jahn, M., Moussa, M., DiMaio, F., 2019. *J. Am. Chem. Soc.* 141 (28), 10948–10952.
- Kaushik, A., Tiwari, S., Jayant, R.D., Marty, A., Nair, M., 2016. *Biosens. Bioelectron.* 75, 254–272.
- Ke, Z., Oton, J., Qu, K., Cortese, M., Zila, V., McKeane, L., Nakane, T., Zivanov, J., Neufeldt, C.H., Cerikan, B., Lu, J.M., Peukes, J., Xiong, X., Kräusslich, H.-G., Scheres, S.H.W., Bartenschlager, R., Briggs, J.A.G., 2020. *Nature* 588 (7838), 498–502.
- Kellner, M.J., Koob, J.G., Gootenberg, J.S., Abudayyeh, O.O., Zhang, F., 2019. *Nat. Protoc.* 14 (10), 2986–3012.
- Lan, J., Ge, J., Yu, J., Shan, S., Zhou, H., Fan, S., Zhang, Q., Shi, X., Wang, Q., Zhang, L., 2020. *Nature* 581 (7807), 215–220.
- Larremore, D.B., Wilder, B., Lester, E., Shehata, S., Burke, J.M., Hay, J.A., Tambe, M., Mina, M.J., Parker, R., 2021. *Sci. Adv.* 7 (1), eabd5393.

- Link, S., El-Sayed, M.A., 1999. Spectral properties and relaxation dynamics of surface plasmon electronic oscillations in gold and silver nanodots and nanorods. *J. Phys. Chem. B* 103 (40), 8410–8426.
- Lisboa Bastos, M., Tavaziva, G., Abidi, S.K., Campbell, J.R., Haraoui, L.-P., Johnston, J. C., Lan, Z., Law, S., MacLean, E., Trajman, A., Menzies, D., Benedetti, A., Ahmad Khan, F., 2020. *BMJ* 370, m2516.
- Midelet, J., El-Sagheer, A.H., Brown, T., Kanaras, A.G., Werts, M.H., 2017. *Part. Part. Syst. Char.* 34 (10), 1700095.
- Mina, M.J., Parker, R., Larremore, D.B., 2020. *N. Engl. J. Med.* 383 (22), e120.
- Mirkin, C.A., Letsinger, R.L., Mucic, R.C., Storhoff, J.J., 1996. *Nature* 382 (6592), 607–609.
- Muyldermans, S., 2013. *Annu. Rev. Biochem.* 82, 775–797.
- Perkins, M.D., Dye, C., Balasegaram, M., Bréchet, C., Mombouli, J.-V., Röttingen, J.-A., Tanner, M., Boehme, C.C., 2017. *Lancet* 390 (10108), 2211–2214.
- Perkins, M.D., Kessel, M., 2015. *Nat. Biotechnol.* 33 (5), 464–469.
- Piebler, J., Schreiber, G., 1999. *J. Mol. Biol.* 289 (1), 57–67.
- Rich, R.L., Cannon, M.J., Jenkins, J., Pandian, P., Sundaram, S., Magyar, R., Brockman, J., Lambert, J., Myszk, D.G., 2008. *Anal. Biochem.* 373 (1), 112–120.
- Robbiani, D.F., Gaebler, C., Muecksch, F., Lorenzi, J.C.C., Wang, Z., Cho, A., Agudelo, M., Barnes, C.O., Gazumyan, A., Finkin, S., Hägglöf, T., Oliveira, T.Y., Viant, C., Hurley, A., Hoffmann, H.-H., Millard, K.G., Kost, R.G., Cipolla, M., Gordon, K., Bianchini, F., Chen, S.T., Ramos, V., Patel, R., Dizon, J., Shimeliovich, I., Mendoza, P., Hartweger, H., Nogueira, L., Pack, M., Horowitz, J., Schmidt, F., Weisblum, Y., Michailidis, E., Ashbrook, A.W., Waltari, E., Pak, J.E., Huey-Tubman, K.E., Koranda, N., Hoffman, P.R., West, A.P., Rice, C.M., Hatzioannou, T., Bjorkman, P.J., Bieniasz, P.D., Caskey, M., Nussenzweig, M.C., 2020. *Nature* 584 (7821), 437–442.
- Sanchez, A., Trappier, S.G., Mahy, B., Peters, C.J., Nichol, S.T., 1996. *Proc. Natl. Acad. Sci. Unit. States Am.* 93 (8), 3602–3607.
- Shubham, S., Hoinka, J., Banerjee, S., Swanson, E., Dillard, J.A., Lennemann, N.J., Przytycka, T.M., Maury, W., Nilsen-Hamilton, M., 2018. *Sci. Rep.* 8 (1), 1–11.
- Stenberg, M., Nygren, H., 1988. *J. Immunol. Methods* 113 (1), 3–15.
- Tang, Y.-W., Schmitz, J.E., Persing, D.H., Stratton, C.W., 2020. *J. Clin. Microbiol.* 58 (6) e00512-00520.
- Thanh, N.T.K., Rosenzweig, Z., 2002. *Anal. Chem.* 74 (7), 1624–1628.
- Trantidou, T., Elani, Y., Parsons, E., Ces, O., 2017. *Microsyst. Nanoengin.* 3 (1), 1–9.
- Wang, Q., Zhang, Y., Wu, L., Niu, S., Song, C., Zhang, Z., Lu, G., Qiao, C., Hu, Y., Yuen, K.-Y., Wang, Q., Zhou, H., Yan, J., Qi, J., 2020. *Cell* 181 (4), 894–904.
- Worldometer, 2021. COVID-19 Coronavirus Pandemic.
- Wu, Y., Wang, F., Shen, C., Peng, W., Li, D., Zhao, C., Li, Z., Li, S., Bi, Y., Yang, Y., Gong, Y., Xiao, H., Fan, Z., Tan, S., Wu, G., Tan, W., Lu, X., Fan, C., Wang, Q., Liu, Y., Zhang, C., Qi, J., Gao, G.F., Gao, F., Liu, L., 2020. *Science* 368 (6496), 1274–1278.
- Zang, F., Su, Z., Zhou, L., Konduru, K., Kaplan, G., Chou, S.Y., 2019. *Adv. Mater.* 31 (30), 1902331.